Indian Journal of Engineering & Materials Sciences
Vol. 32, December 2025, pp. 684-693
DOI: 10.56042/ijems.v32i06.24024

Design, simulation, and experimental validation of a corrugated morphing airfoil actuated by SMA-Spring mechanism

Kartikeya Parmar[a], Palani Anand Iyamperumal[a] & Santhanam Ranganathan[b]

[a]IIT Indore, 453 552, India

[b]DRDL, Hyderabad 500 058, India

Received: 20 September 2025; accepted: 02 December 2025

This research paper has presented the design, numerical analysis, and experimental validation of a bio-inspired morphing airfoil actuated through shape memory alloy (SMA) wire and spring elements. To facilitate controlled deflection, a corrugated morphing section has been embedded within an eppler airfoil, which has been selected through comparative aerodynamic analysis against a standard NACA 0012 profile. Finite element simulations have been conducted using ANSYS software to investigate tip deflection performance across varying morphing region lengths and actuator placements. A lightweight, three-dimensionally printed prototype incorporating shape memory alloy components has been developed and has been thoroughly evaluated using direct electrical heating methods. Experimental findings have shown a 4 mm downward deflection for a 1 mm actuator wire contraction, which has closely matched the numerical simulation predictions. To demonstrate scalability, a full-span wing prototype has been assembled utilizing three independent, actuated airfoil segments. The successful actuation of this system has validated the feasibility of shape memory alloy-driven morphing as a viable, lightweight alternative to traditional servo-based mechanisms in micro air vehicles and low-speed unmanned aerial vehicles. Furthermore, this research has established a practical foundation for future work aimed at enabling bi-directional actuation for enhanced aerodynamic control and maneuverability.

Keywords: Additive manufacturing, Finite element analysis, Micro air vehicles, NiTi alloys, Smart structures, Variable camber

1 Introduction

Unmanned aerial vehicles (UAVs) and micro aerial vehicles (MAVs) have experienced rapid advancements over the last decade, driving the need for lightweight, compact, and energy-efficient actuation systems Hassanalian[1], Floreano[2]. Conventional flight control architectures in these platforms primarily rely on servo motors to operate control surfaces such as ailerons, elevators, rudders, or morphing sections. While servo motors provide precision and responsiveness, their drawbacks—added mass, mechanical complexity, noise, and high power consumption—become particularly limiting in small-scale aerial vehicles, where every gram and watt matter Sofla[3], Jani[4]. To overcome these challenges, researchers have explored the use of smart materials, particularly shape memory alloys (SMAs), which can undergo significant deformation and return to their original shape upon thermal activation. Nickel–Titanium (NiTi) alloys, a prominent class of SMAs, exhibit unique thermomechanical behaviors such as the shape memory effect and pseudoelasticity Sun[5], Leary[6]. These features enable compact, silent, and mechanically simple actuation without conventional moving parts, making SMAs attractive candidates for morphing applications in aerospace. Prior studies have demonstrated the feasibility of SMA-based actuation in morphing wings, deployable aerospace components, and adaptive structures Borghetti[7], Rodrigue[8].

Several designs have shown the aerodynamic advantages of SMA-driven morphing systems. An SMA-actuated airfoil with a super elastic skin that enabled continuous shape variation and improved lift characteristics has been developed, Barbarino[9]. Ko[10] demonstrated a high-lift morphing wing using embedded SMA actuators under low-speed conditions. Beyond actuation mechanisms, structural innovations such as corrugated skins have been introduced to enhance flexibility and reduce bending stiffness Thill[11], Yokozeki[12]. Bai[13] proposed a corrugated morphing skin for UAV wings, offering improved adaptability, and Liu[14]advanced a bio-inspired antagonistic SMA wire configuration that enabled multi-directional morphing. Additional research has explored similar lightweight architectures

*Corresponding author (E-mail: Phd2301103009@iiti.ac.in)

to optimize control surface responsiveness in small-scale aircraft Ashir[15], Almedia[16]. These studies highlight the potential of combining SMAs with structural tailoring to achieve efficient morphing behavior.

However, many existing approaches depend on complex linkages or multi-layered SMA arrays, which increase weight and integration difficulties Karagiannis[17], Kouchlef[18]. Furthermore, bidirectional actuation often requires antagonistic actuator arrangements or hybrid material systems, adding to system complexity Martinez[19]. Detailed investigations into material fatigue have further suggested that simplified routing can improve actuator longevity in MAV applications Aly[20]. To address these limitations, the present study introduces a simplified SMA-based morphing concept wherein a pre-stretched SMA spring actuates a wire routed through a corrugated airfoil. The contraction force generated by the SMA spring is transmitted to the trailing edge via the embedded wire, producing meaningful deflection with minimal mass and power requirements. This design leverages the advantages of corrugated geometries for flexibility while maintaining mechanical simplicity.

A prototype corrugated Eppler airfoil (200 mm chord, 50 mm thickness) has been fabricated using 3D printing to validate this concept. Finite Element simulations in ANSYS have demonstrated that a 1 mm contraction of the actuation wire could generate a trailing-edge deflection of approximately 4 mm, confirming the feasibility of the approach. This paper has presented the aerodynamic evaluation, structural modeling, and experimental validation of the proposed morphing mechanism. The objective is to establish a practical, scalable, and low-cost morphing solution for energy-efficient UAVs and MAVs, while also laying the groundwork for future bi-directional actuation systems.

2 Materials and Methods

2.1 Aerodynamic analysis

Before implementing the morphing mechanism, it was essential to identify an airfoil geometry with aerodynamic characteristics suited to low-speed UAV and MAV operations. A comparative computational fluid dynamics (CFD) analysis was therefore performed between the symmetric NACA 0012 airfoil, which is widely used as a baseline in aerodynamic studies, and the Eppler airfoil, which is designed to provide higher lift at low Reynolds numbers.

2.1.1 Computational domain and boundary setup

Both airfoil geometries were constructed in Autodesk Fusion 360 with a chord length of 1 m, and imported into ANSYS Fluent for CFD analysis. The flow domain consisted of a C-shaped enclosure with a 7.5 m radius from the airfoil center and extended wall boundaries of 15 m, as illustrated in Fig. 1a. The mesh was generated with unstructured triangular elements, including inflation layers near the airfoil surface to accurately resolve boundary layer effects Fig. 1b. The computational domain was defined with specific boundary conditions to ensure accurate representation of the aerodynamic environment. A uniform velocity of 6 m/s was applied at the inlet, while the outlet was configured as a pressure outlet with a gauge pressure of 0 Pa. A no-slip condition was implemented for both the airfoil surface and the domain walls. The working fluid, air, was characterized by a constant density of 1 kg/m³ and a kinematic viscosity of 10^{-6} m²/s. Furthermore, the Spalart–Allmaras turbulence model was utilized for the study, as it is a widely accepted standard for external aerodynamic simulations.

2.1.2 Angle of attack variation and data collection

The angle of attack (AoA) was systematically varied from 0° to 20° in incremental steps for both

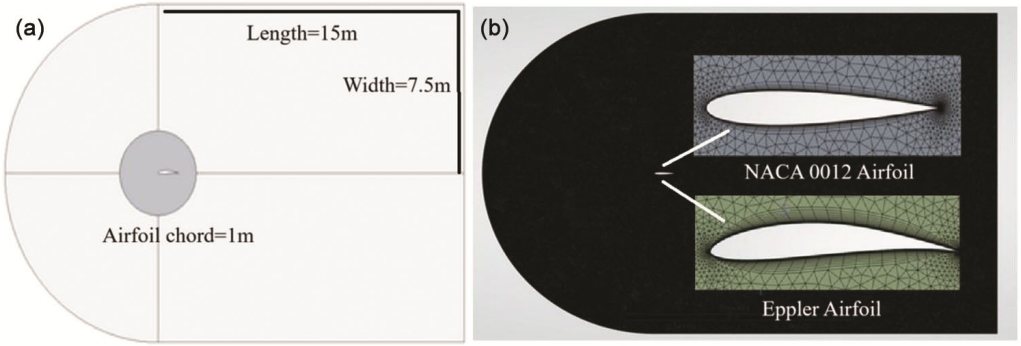

Fig. 1 — (a) Computational domain and (b) Mesh topology for CFD simulation of airfoil geometries.

airfoil configurations. For each AoA, the aerodynamic coefficients—including lift coefficient (C_l), drag coefficient (C_d), and the lift-to-drag ratio (C_l/C_d)—were computed.

2.2 Structural simulation of the SMA-Actuated eppler airfoil

2.2.1 Finite element model description

To evaluate the structural response of the proposed SMA-spring-driven morphing airfoil, a static structural analysis was carried out using ANSYS Workbench. Initially a comparison study is made with airfoil section of length 1000 mm and deflection is compared. Later on the airfoil was modeled with scaled dimensions as mentioned in Table 1, incorporating a corrugated internal structure with predefined holes for routing the actuation wire. The purpose of the corrugation was to reduce weight while maintaining bending stiffness and facilitating internal actuation.

A SMA wire of 1 mm diameter and 35 mm length was inserted through the internal holes at a location approximately 5 mm above the lower surface (base) of the airfoil. This wire acts as the medium for transferring contraction force from an external SMA spring to the trailing edge of the airfoil. The actuation was simulated by applying a 1 mm axial displacement at the wire end (mimicking SMA spring contraction) (Fig. 2).

2.2.2 Material properties

The material properties for the simulation are summarized in Table 2.

The materials were treated as linearly elastic and isotropic for simplicity, given the low-displacement regime being studied.

2.2.3 Boundary conditions and meshing

The leading edge of the airfoil was fixed in all degrees of freedom to represent a cantilever configuration. The wire was connected rigidly to the trailing edge structure, ensuring that any axial movement would transfer bending to the airfoil. The wire end was assigned a 1 mm displacement in the axial direction. Tetrahedral meshing with local refinement near the wire was used to ensure accuracy in stress and deformation zones.

2.3 Parametric optimization of the morphing mechanism

Following the validation of the morphing mechanism through structural simulation, a

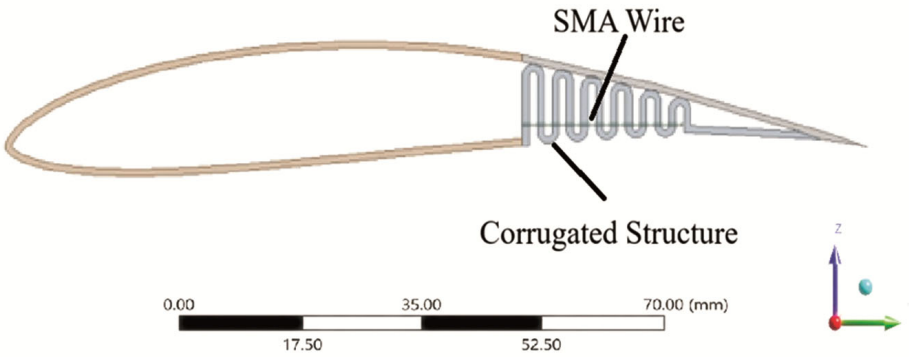

Fig. 2 — Cross-sectional view of the 3D model of the morphing airfoil with a corrugated trailing-edge section. The internal channel accommodates a 1 mm sma wire positioned 5–7 mm from the base, which is displaced by an SMA spring for actuation.

Table 1 — Dimensional comparison between the reference airfoil and the scaled prototype.

Chord	Reference dimension[20]	Scaled prototype
Thickness	1000 mm	200 mm
Length of wire	150 mm	35 mm
Diameter of splined section	25 mm	5 mm
Length of unmorphed section	600 mm	120 mm
Length of morphed section	400 mm	80 mm
Thickness of splined section	8 mm	1.6 mm

Table 2 — Material properties of the airfoil and actuation wire used in the structural simulation.

Airfoil	Carbon Fiber Reinforced Polymer (CFRP)	Young's Modulus: 70 GPa	Poisson's Ratio: 0.3	Density: 1600 kg/m³
Wire	Shape memory alloy(SMA) wire	Young's Modulus: 200 GPa	Poisson's Ratio: 0.3	Density: 6450 kg/m³

systematic parametric study was undertaken to investigate the influence of actuator placement, displacement magnitude, material selection, and corrugated section thickness on trailing-edge deflection.

2.3.1 Effect of wire position

To investigate the influence of actuator placement on structural deformation, a parametric study was performed by varying the vertical position of the wire within the corrugated carbon fiber airfoil. The goal was to identify the optimal location that maximizes trailing edge deflection when a fixed horizontal displacement is applied to the embedded wire.

The sma wire used had a diameter of 1 mm and a length of approximately 35 mm. A displacement of 1 mm was applied at the free end of the wire, while the base of the airfoil remained fixed. The simulations were carried out in ANSYS (Fig. 3), and tip deflection was measured at the trailing edge.

A range of wire positions was studied, from 3 mm to 9 mm above the airfoil base

2.3.2 Effect of wire material

In this study, the influence of actuator wire material on airfoil deflection was evaluated by replacing the sma wire with titanium and copper. The displacement applied at the tip of the wire was fixed at 1 mm in all cases, simulating the actuation of a smart material (e.g., SMA spring).

2.3.3 Effect of input displacement

A parametric analysis was conducted to study the effect of varying input displacement applied to the actuator wire while keeping its position (4 mm from base) and material (SMA) constant. The applied displacements were set to 0.5 mm, 1.0 mm, 1.5 mm, and 2.0 mm.

2.3.4 **Effect of corrugated section thickness**

To investigate the influence of structural stiffness on actuation performance, a parametric study was conducted by varying the thickness of the corrugated trailing section while maintaining constant material properties and input displacement (1 mm).

2.4 Experimental materials and methods

To validate the simulation results and demonstrate the practical implementation of the proposed morphing airfoil concept, an experimental setup was developed using shape memory alloy (SMA) springs and a 3D printed Eppler airfoil model as shown in Fig. 4.

2.4.1 Experimental setup

A lightweight airfoil model of 200 mm chord length and 50 mm thickness was 3D printed using PLA material, incorporating a corrugated trailing edge structure. A sma wire (Ø 1 mm, L = 35 mm) was embedded in the corrugated section, and an SMA spring (compressed length 2 cm, extended length 11 cm, Ø0.2 mm) was mechanically linked to this wire. The SMA spring was actuated using a variable DC power supply, and a brass connector was used to join the SMA spring to the sma wire. The spring contracted upon heating due to resistive heating, pulling the wire and causing a deflection at the trailing edge.

A scale was fixed at the airfoil tip to measure deflection. A temperature sensor (LM35) was used to monitor surface temperature, and a laser displacement sensor is proposed for future implementation to measure deflection with higher precision.

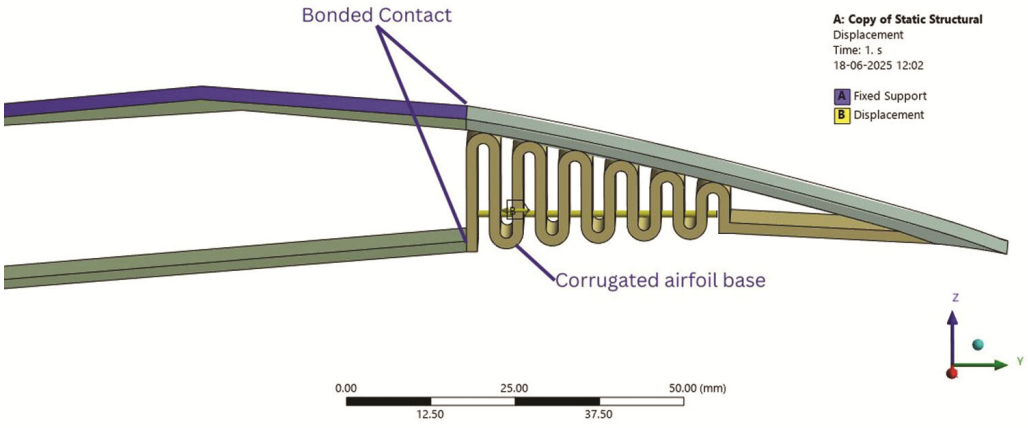

Fig. 3 — Simulation boundary conditions applied in ANSYS. The leading edge is fixed, while a 1 mm displacement is applied at the end of the sma wire located 4 mm from the base.

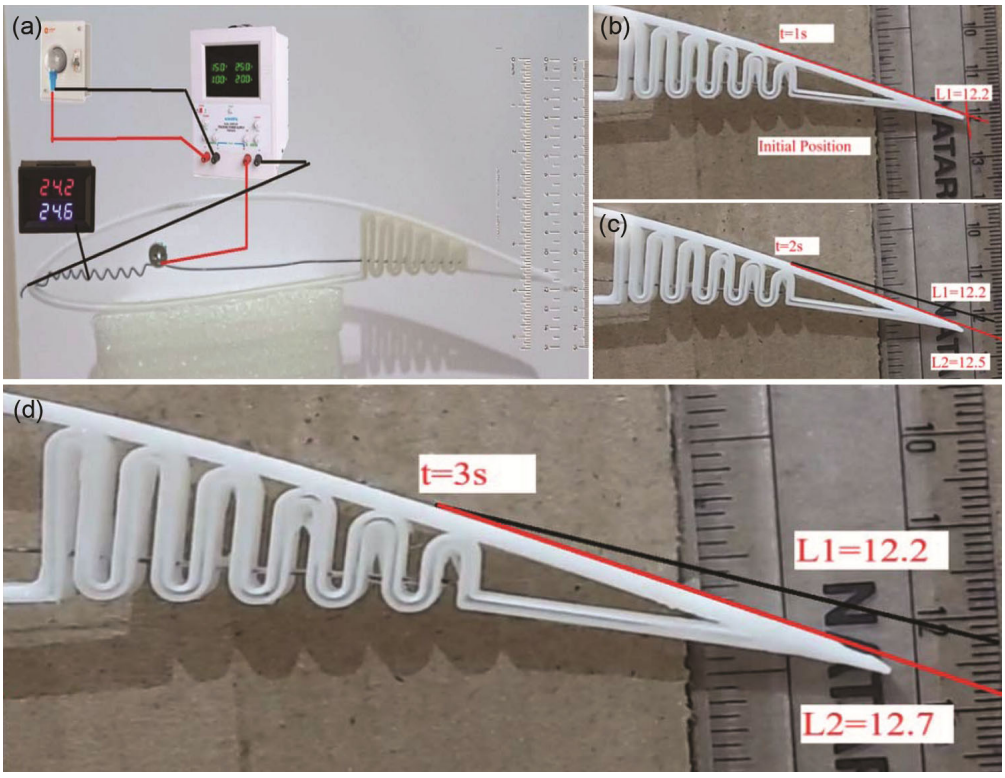

Fig. 4 — Photograph of the experimental setup (a) Power supply & circuit, (b) Initial position, (c) Intermediate deflection and (d) Final deflection at t=3s.

3 Results and Discussion

3.1 Aerodynamic results

3.1.1 Result discussion (lift, drag, Cl/Cd comparison Eppler vs NACA)

As shown in the Fig. 5, the Eppler airfoil outperforms the NACA 0012 airfoil in terms of lift across the full range of AoA tested. At 2° AoA, the Eppler reaches a C_l of 0.8998, while the NACA 0012 achieves only 0.216. Even at higher AoA, the Eppler airfoil maintains high lift without abrupt stall, reaching a peak C_l of 1.85 at 14°, followed by a gradual decrease.

While the Eppler airfoil exhibits slightly higher drag, the C_l/C_d ratio remains significantly superior to the NACA 0012 profile up to 16° AoA, demonstrating better aerodynamic efficiency a key advantage when used in morphing wing systems with limited actuation force such as SMA springs.

Based on this analysis, the Eppler profile was selected as the baseline for further simulation, structural deformation studies, and experimental morphing implementation.

The Eppler airfoil exhibits significantly higher lift and favorable C_l/C_d ratios compared to the symmetric NACA 0012, validating its use in morphing wing design under low-speed conditions

3.2 Structural simulation results

3.2.1 Results and discussion (4 mm deflection for 1 mm stroke, stress analysis)

The simulation showed that the applied displacement at the wire end resulted in an downward tip deflection of approximately 4.06 mm at the trailing edge (Fig. 6). The deformation was localized toward the aft region of the airfoil, as expected, with minimal movement near the fixed leading edge. The stress concentration was observed along the path of the embedded wire, with maximum Von Mises stress well within the elastic limits of both the wire and airfoil material, indicating structural safety. These results confirm that a small displacement (1 mm) through an SMA spring can produce meaningful morphing (~4 mm tip deflection), which could be sufficient for minor control surface adjustments in UAVs or adaptive wings.

The simulation validates the feasibility of using an SMA spring–SMA wire combination for passive and lightweight morphing actuation. A parametric study and further analysis are done to evaluate the effect of

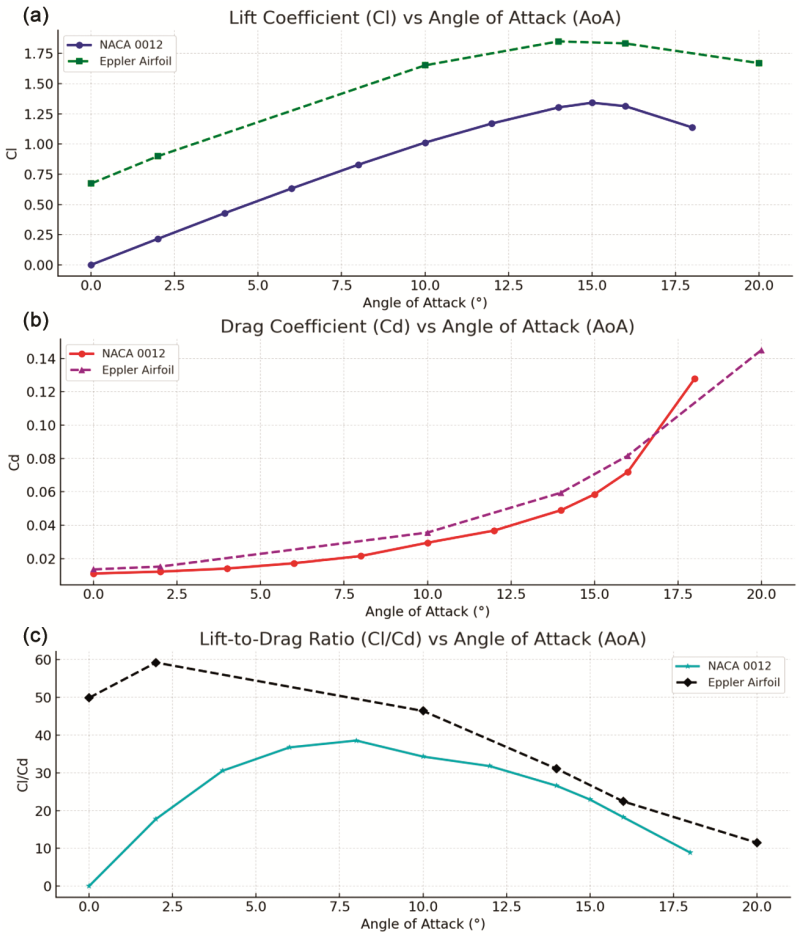

Fig. 5 — Aerodynamic performance comparison between NACA 0012 and eppler airfoil (a) Lift coefficient (C_l) vs angle of attack, (b) Drag coefficient (C_d) vs angle of attack and (c) Lift-to-drag ratio (C_l/C_d) vs angle of attack.

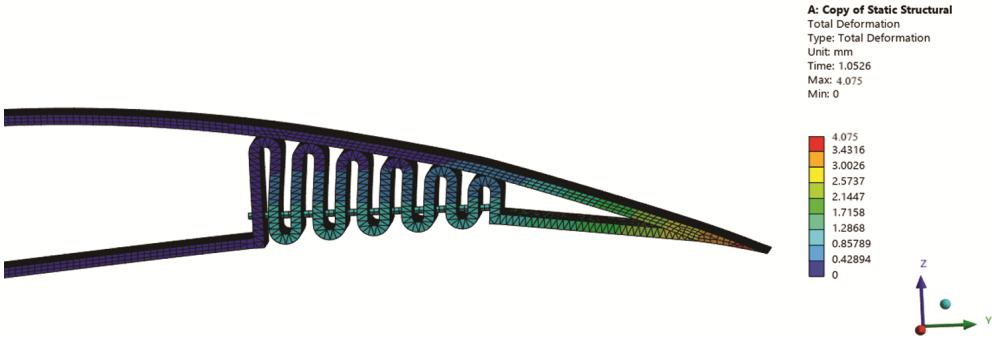

Fig. 6 — Total deformation contour of the airfoil under 1 mm displacement applied to the sma wire at 4 mm from the base. The trailing edge shows a maximum deflection of approximately 4.06 mm.

displacement magnitude, actuation force, and material choice on the morphing efficiency and structural behavior.

3.2.2 Effect of wire position

A range of wire positions was studied, from 3 mm to 9 mm above the airfoil base. The observed tip deflections are summarized in Table 3.

A second-degree polynomial curve was fitted to the data to analyze the trend. The deflection initially increases with wire position, reaching a maximum at 4.06 mm, and then gradually decreases. This behavior is consistent with mechanical principles—lower wire placements near the airfoil base provide better leverage and result in higher moment-induced tip displacement.

Table 3 — Effect of wire position on tip deflection of the airfoil.

Wire position from base(mm)	Tip deflection(mm)
3	3.93
4	4.06
5	4.02
6	3.93
7	3.61
8	2.97
9	1.96

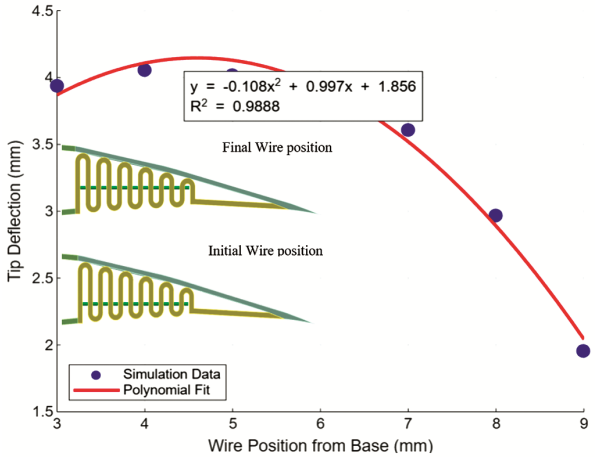

Fig. 7 — Effect of wire position on airfoil tip deflection. A second-order polynomial fit indicates that the maximum deflection of 4.06 mm occurs at 4 mm wire position from the base. The fitted curve helps visualize the nonlinear behavior of structural deflection with varying actuator placement.

The results demonstrate that there is a clear nonlinear relationship between wire placement and deflection response. The optimal actuator location was found to be 4 mm from the base, yielding a maximum tip deflection of 4.06 mm. These findings are physically consistent and align well with expected structural behavior under bending loads. A graphical representation of the deflection trend with polynomial fitting is provided in Fig. 7

3.2.3 Effect of wire material

The simulated tip deflections for different wire materials are summarized in Table 4. This result simplifies the actuator selection process, suggesting that materials may be chosen based on other criteria such as weight, fatigue resistance, or cost, without adversely affecting deflection performance under fixed displacement. While the deflection response is primarily determined by the routing geometry and displacement magnitude, SMA wire has been selected for the final prototype to ensure better functional compatibility with the SMA spring actuator. Furthermore, preliminary structural observations

Table 4 — Comparison of airfoil tip deflection with various actuator wire materials under 1 mm displacement.

Material	Young's Modulus (GPa)	Tip Deflection (mm)
Sma wire	200	4.06
Titanium	116	~4.06
Copper	110	~4.06

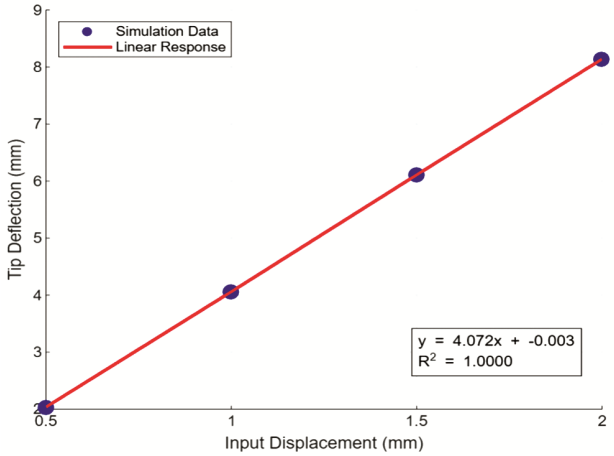

Fig. 8 — Variation of airfoil tip deflection with actuator wire displacement. The linear response confirms the elastic behavior of the structure in the tested displacement range, simplifying prediction and control of deformation.

indicate that the high flexibility of SMA wires facilitates a more uniform stress distribution within the thin corrugated walls compared to rigid metallic alternatives, thereby enhancing the fatigue life of the morphing section under cyclic loading

3.2.4 Effect of wire displacement

The results indicate a nearly linear increase in tip deflection with increasing actuator displacement (Fig. 8). For instance, a displacement of 1 mm caused a tip deflection of 4.06 mm, while doubling the input to 2 mm led to a deflection of 8.14 mm. This confirms that the structure exhibits linear elastic behaviour in the tested range, and the deflection output is directly proportional to actuator displacement.

This observation is beneficial for design purposes, as it simplifies control and prediction of airfoil deformation under different actuation levels. The deflection-displacement relationship is shown in Fig. 8.

3.2.5 Effect of section thickness

The baseline thickness of 1.6 mm yielded a tip deflection of 4.06 mm. Reducing the wall thickness to 0.75 mm and 0.5 mm increased the deflection to 4.29 mm and 4.64 mm, respectively, due to reduced bending stiffness. However, a further reduction to 0.25 mm resulted in a decrease in deflection

(4.16 mm), likely due to local instability and geometric nonlinearities at very thin walls. These results shown in Fig. 9 suggest that while thinner structures enhance flexibility, there exists a lower threshold beyond which structural response may deteriorate or destabilize.

3.3 Experimental results

The experimental procedure involved applying incremental voltages ranging from 1.23 V to 2.0 V and recording the duration required for the SMA spring to reach full actuation. At each specific voltage level, the actuation time and the resulting tip deflection were recorded manually. Initial observations indicated that at an applied voltage of 1.23 V, the actuation time was 240 s with a minimal recorded deflection of approximately 0.5 mm. In contrast, increasing the voltage to 2.0 V resulted in full spring actuation within 10 s, yielding a maximum tip deflection of approximately 4 mm. These experimental values have been plotted to illustrate the relationship between voltage and actuation time (Fig. 10a) as well as a comparative analysis of experimental versus simulated tip deflection (Fig. 10b)

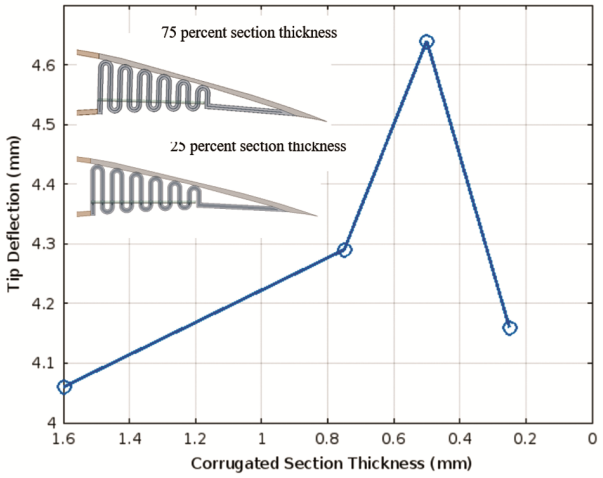

Fig. 9 — Variation of tip deflection with respect to corrugated section thickness. A nonlinear increase in deflection is observed, followed by a drop at ultra-thin sections due to potential instability.

3.4 Prototype demonstration of SMA driven morphing wing

To validate the practicality of the proposed morphing airfoil concept, a full-span wing prototype was fabricated by symmetrically integrating three SMA-actuated corrugated airfoils along a 40 cm blade length. Each airfoil segment incorporates a morphing section driven by embedded Shape Memory Alloy (SMA) components—namely, an SMA wire and a pre-stretched SMA spring. The prototype was constructed using lightweight materials and 3D-printed parts, with the SMA components positioned within the trailing-edge region to induce downward deflection upon heating. The actuation mechanism was powered using a direct current supply, and the initial tests demonstrated a downward deflection of approximately 4 mm for a 1 mm contraction in SMA wire length, consistent with earlier simulation findings. Figure 11 presents the side profile highlighting the corrugated geometry and internal SMA integration. This demonstrator validates the feasibility of employing SMA for distributed morphing without relying on traditional servomechanisms. Moreover, the current arrangement offers a scalable solution for lightweight morphing

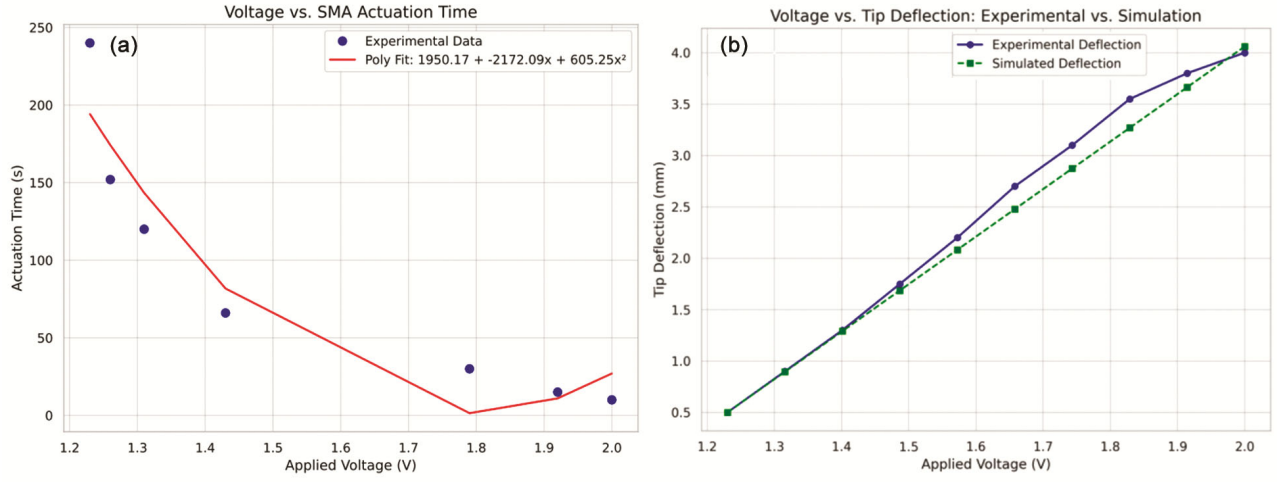

Fig. 10 — (a) Plot showing the reduction in actuation time with increasing voltage applied to the SMA spring and (b) Comparison of simulated and experimental tip deflection data as a function of applied voltage.

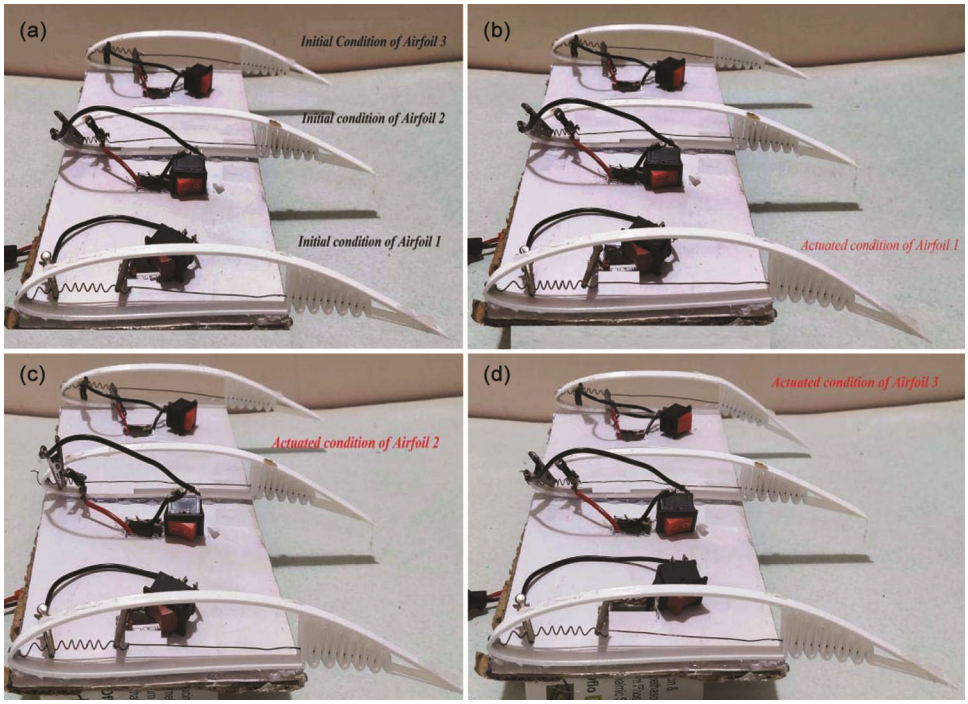

Fig. 11 — (a) Side view of initial configuration and sequential actuation of (b) Airfoil 1, (c) Airfoil 2 and (d) Airfoil 3.

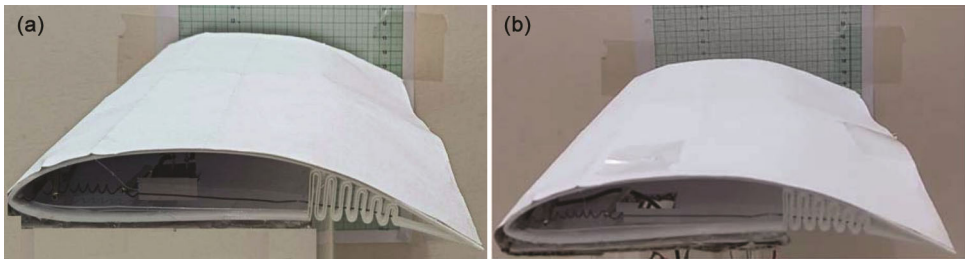

Fig. 12 — Fabricated SMA-driven morphing wing in (a) unactuated and (b) actuated states. The deformation of ~5 mm at the trailing edge confirms the viability of SMA springs for distributed morphing with minimal weight and compact integration.

systems applicable to Micro Air Vehicles (MAVs) and bio-inspired UAV platforms. Future development will focus on enabling bi-directional actuation through antagonistic SMA configurations and achieving complete in-flight demonstration. The successful realization of this prototype marks a significant step toward compact, power-efficient, and mechanically simple morphing wing architectures.

To further demonstrate the coordinated response of the entire morphing wing, all three airfoils were simultaneously actuated after successful individual testing. Each airfoil segment responded uniformly to the applied thermal stimulus, resulting in a continuous and smooth deformation along the full wing span. The SMA springs, upon heating, effectively contracted the embedded SMA wires, leading to a measurable trailing-edge deflection across all segments. This full-span actuation validated the synchronization of the distributed SMA mechanism and reinforced the potential of the proposed system for integrated wing morphing. Figure 12 illustrates the wing before and after actuation, highlighting the achieved deflection and the operational integrity of the SMA-driven structure under coordinated excitation.

4 Conclusion

This study successfully demonstrates the design, simulation, and physical prototyping of a novel morphing airfoil actuated by Shape Memory Alloy (SMA) wires integrated within a corrugated structure. Through detailed finite element analysis and experimental validation, it was observed that SMA-induced contraction can produce up to 4 mm downward deflection for a 1 mm actuator stroke, highlighting the structure's high mechanical advantage. The fabricated prototype, composed of

three airfoil segments aligned along a 40 cm blade span, confirmed the feasibility of SMA wire actuation in achieving smooth and continuous morphing without external hinges or bulky servomotors.

The system was experimentally validated using embedded SMA wires and springs, which successfully reproduced the simulated deflection profile, showcasing the practical application of smart materials in lightweight morphing systems. This design approach paves the way for the development of compact, adaptive air structures with enhanced aerodynamic performance.

Future Work: Building upon this foundation, current research efforts are focused on enabling bidirectional actuation of the morphing airfoil. To achieve this, SMA springs are being explored in angled configurations to induce upward deflection upon activation. Simulation results using inclined SMA wires have already shown promising upward displacement of up to 3 mm, and experimental validation is in progress. Additional parametric studies involving spring angle, placement geometry, and actuator length are being conducted to optimize performance.

In the next phase, these enhancements will be integrated into a full-span, fully-actuated morphing wing to enable pitch control and active shape adaptation in micro air vehicles (MAVs). This work lays the groundwork for scalable morphing solutions and establishes a viable pathway for replacing traditional actuation systems with embedded smart material technologies in aerospace applications.

References

1 Hassanalian M & Abdelkefi A, *Prog Aerosp Sci*, 91 (2017) 99.
2 Floreano D & Wood R J, *Nature*, 521 (2015) 460
3 Sofla A Y, Meguid S A, Tan K T & Yeo W K, *Smart Mater Struct*, 19 (2010) 073001.
4 Jani J M, Leary M, Subic A & Gibson M A, *Mater Des*, 56 (2014) 1078.
5 Sun L, Huang W M, Ding Z, Zhao Y, Wang C C, Purnawali H & Tang C, *Mater Des*, 33 (2012) 577.
6 Mohd Jani J, Leary M, Subic A & Gibson M A, *Mater Des*, 56 (2014) 1078.
7 Borghetti F, Canziani F, Riva G, & Belingardi G, *Aerospace*, 7 (2020) 62.
8 Rodrigue H, Wei W, Bhandari B & Ahn S H, J Mech Sci Technol, 28 (2014) 4581.
9 Barbarino S, Pecora R, Lecce L V, Concilio A, Ameduri S & Calvi E, *J Mater Eng Perform*, 18 (2009) 696.
10 Ko S H, Bae J S & Rho J H, *Smart Mater Struct*, 23 (2014) 085008.
11 Thill C, Etches J, Bond I, Potter K & Weaver P, *Aeronaut J*, 112 (2008) 117.
12 Yokozeki T, Takeda S I, Ogasawara T & Ishikawa T, *Compos Part A Appl Sci Manuf*, 37 (2006) 1578
13 Bai J B, Chen D, Xiong J & Shenoi R, *Compos Part B Eng*, 131 (2017) 134.
14 Yang J, Zhang Y, Gu X, Li J, Fang P, Yang X, Wang J, Zhu J & Zhang W, *Chin J Aeronaut*, 37 (2024) 373.
15 Ashir M, Hindahl J, Nocke A & Cherif C, *J Ind Text*, 50 (2019) 114
16 Almeida T, Santos O & Otubo J, *J Aerosp Technol Manag*, 7 (2015) 454
17 Karagiannis D, Stamatelos D, Spathopoulos T, Solomou A, Machairas T, Chrysohoidis N, Saravanos D & Kappatos V, *Aircr Eng Aerosp Technol*, 86 (2014) 10.
18 Kouchlef M & Xing S, *Int J Sci Res Arch*, 12 (2024) 800.
19 Martinez J M, Scopelliti D, Bil C, Carrese R, Marzocca P, Cestino E & Frulla G, *AIAA Paper*, (2017) 0059
20 Aly R, Kaygan E & Esat V, *Int J Aeronaut Space Sci*, 26 (2025) 562